Available online at www.sciencedirect.com

SciVerse ScienceDirect

Ceramics International 38 (2012) 6671–6676

CERAMICS INTERNATIONAL

www.elsevier.com/locate/ceramint

Effect of chromium addition on the structural, morphological and magnetic properties of nano-crystalline cobalt ferrite system

Yüksel Köseoğlu[a,*], Mousa Ibrahim Oleiwi Oleiwi[a], Resul Yilgin[b], Abdullah N. Koçbay[b]

[a]*Department of Physics, Fatih University, Buyukcekmece, 34500 İstanbul, Turkey*
[b]*Department of Physics, Gebze Institute of Technology, Cayirova, 41400 Kocaeli, Turkey*

Received 21 March 2012; received in revised form 15 May 2012; accepted 17 May 2012
Available online 26 May 2012

Abstract

Nano-crystalline chromium doped cobalt ferrite powders have been synthesized by PEG assisted hydrothermal route. The structural, morphological and magnetic properties of the products were determined by X-ray diffraction (XRD), scanning electron microscopy (SEM), energy-dispersive X-ray (EDX) spectroscopy and vibrating sample magnetometer (VSM). X-ray analysis showed that the samples were cubic spinel. SEM images reveal that the samples' surfaces exhibit well-defined crystalline nanoparticles of spherical shapes with small agglomeration. The addition of Cr^{3+} ions caused a decrease in the average crystallite size, magnetization and the coercive field of the sample. The observed decreases in saturation magnetization and coercivity are explained on the bases of exchange interactions.

Keywords: Hydrothermal synthesis; XRD; Magnetic nanoparticles; Mn–Co spinel ferrites

1. Introduction

Magnetic nanostructured materials have gained great interest of the scientists due to their unusual physical properties compared to their bulk form. They have very large areas of applications in technology, such as electronic devices, microwave devices, transformer cores, magnetic devices, switching devices, recording tapes, permanent magnets, hard disc recording media, flexible recording media, read–write heads, active components of ferrofluids, magnetic drug delivery, catalysis, color imaging, magnetic refrigeration, detoxification of biological fluids, magnetically controlled transport of anti-cancer drugs, magnetic resonance imaging (MRI) contrast enhancement and magnetic cell separation, etc [1–18].

The ferrite nanoparticles have a spinel structure and the general spinel structure is in the form as AB_2O_4. Cobalt ferrite, $CoFe_2O_4$, is a partially inverted spinel structure with cobalt atoms predominantly in the octahedral sites [19] and it is a well-known hard magnetic material, which has been studied in detail due to its high coercivity (5400 Oe), high chemical stability, good electrical insulation, significant mechanical hardness and moderate saturation magnetization (~80 emu/g) at room temperature. However, in the case of $CoFe_2O_4$ nanoparticles, magnetic and electrical properties are much different than those in the bulk form and variation of these properties with the size and synthesis methods have been reported [20–23].

Since the past decades, various synthesis methods have been used for the preparation of nanocrystalline magnetic materials. Some of them are mechanical-milling, co-precipitation, microwave assisted route, reverse and normal micelles, reflux method, oxidation–reduction method, sol–gel method, micro emulsion method, and thermal decomposition method [23–25]. And there are some advantages and disadvantages during the production processes because of the time consumption, cost, crystallinity and morphology of the nanoparticles.

The properties of ferrite nanoparticles are influenced by composition and microstructure. The addition of impurities induces changes in the defect structure and texture of the crystal, creating significant modifications in the magnetic and electrical properties of these materials. Addition

*Corresponding author. Tel.: +90 212 8663300; fax: +90 212 8663402.
E-mail address: yukselk@fatih.edu.tr (Y. Köseoğlu).

0272-8842/$36.00 © 2012 Elsevier Ltd and Techna Group S.r.l. All rights reserved.
http://dx.doi.org/10.1016/j.ceramint.2012.05.055

of Cr^{3+} ions could produce sufficient changes in $A[B_2]O_4$ structure and known that Cr^{3+} ions have strong B-site preference. Since Cr^{3+} ($3\ \mu_B$) has a weaker magnetic moment than Fe^{3+} ($5\ \mu_B$), the partial replacement of Fe^{3+} by Cr^{3+} ion will cause a decrease in saturation magnetization and coercivity of the sample. Several researchers have studied the effects of Cr substitution in the spinel ferrites [26–28]. However, we could not find any reports related to hydrothermal synthesis and magnetic properties in the literature on Cr substituted cobalt ferrites.

In our study, we have successfully synthesized Cr doped $CoFe_2O_4$ nanoparticles by using polyethylene glycol (PEG)—assisted hydrothermal method which is cheap and easy to get a good result. The method of hydrothermal synthesis is processing at high pressure and low temperature at around 180 °C. Hydrothermal processing can be defined as any homogeneous (nanoparticles) or heterogeneous (bulk materials) reaction in the presence of aqueous solvents or mineralizers under high pressure and low temperature conditions to dissolve and recrystallize (recover) materials that are relatively insoluble under ordinary conditions [29–31]. During the synthesis we used low-cost coating material PEG as the surfactant which is one of the polymers with major interest in this area because it is non-toxic, non-flammable and easy to handle. Various morphologies with different sizes and shapes can be obtained by PEG-coating. It is verified that using PEG is very advantageous to prevent agglomerations and to obtain small particle sizes with good crystallinity as emphasized in different works [30,31].

X-ray powder diffractometer (XRD), Fourier transform infrared spectroscopy (FTIR), transmission electron microscopy (TEM) and vibrating sample magnetometer (VSM) were used for the structural, morphological and magnetic investigation of the products, respectively.

2. Experimental

2.1. Synthesis

To prepare Cr doped $CoFe_2O_4$ nanoparticles (NPs), in an appropriate ratio, stoichiometric molar amounts of chromium nitrate $[Cr(NO_3)_3 \cdot 9H_2O]$, ferric nitrate $[Fe(NO_3)_3 \cdot 9H_2O]$ and cobalt nitrate $[Co(NO_3)_2 \cdot 6H_2O]$ were each dissolved in 10 mL of distilled water to form a clear solution and mixed altogether. The mixture was stirred with a magnetic stirrer until the reactants were dissolved completely. During the stirring, 10 mL PEG-400 was added to the solution to serve as a surfactant that covers NPs and prevents agglomeration. And then pH of the solution was adjusted to 11.0 by adding 2 M NaOH drop-by-drop. After continuous stirring at 400 rpm for an hour, a homogeneous solution could be obtained. The obtained solutions were put into the autoclaves up to two thirds of their total volume (50 mL). Lastly, the autoclaves were left in an oven at 180 °C for 24 h and then were allowed to cool to room temperature. The products were centrifuged and washed several times with de-ionized water, acetone and absolute ethanol. Then the samples were put again in an oven at 70 °C to dry. Taken solid phase samples were ground in a mortar to powder them. Obtained powders were used for all of the measurements.

2.2. Measurements

X-ray powder diffraction analysis was conducted on a Huber JSO-DEBYEFLEX 1001 Diffractometer (XRD) using Cu K_α (operated at 40 kV and 35 mA).

FTIR transmission spectra were taken on Mattson Satellite Infrared Spectrometer from 4000 to 400 cm^{-1}.

Field Emission Scanning Electron Microscope (FE-SEM, JEOL 7001 FE with EDX) was used in order to investigate the nanostructure morphology and elemental composition of the samples. The samples were coated with carbon prior to SEM analysis.

Room temperature magnetic measurements were carried out with the Quantum Design Model 6000 Vibrating Sample Magnetometer (VSM) option for the Physical Property Measurement System (PPMS) and parameters like specific saturation magnetization (M_s), coercive force (H_c) and remanence (M_r) were evaluated.

3. Results and discussion

3.1. XRD analysis

X- ray diffraction study of all the samples confirmed the formation of single phase cubic spinel structure. Typical microphotographs of undoped ($CoFe_2O_4$) and chromium doped ($CoCr_{0.3}Fe_{1.7}O_4$) samples are presented in Fig. 1. The average crystallite sizes were calculated by Scherer's equation (Eq. (1)) from the reflection of the spinel structure's $d_{(311)}$ plane.

$$D_{XRD} = 0.9\lambda/\{\beta \cos \theta\} \quad (1)$$

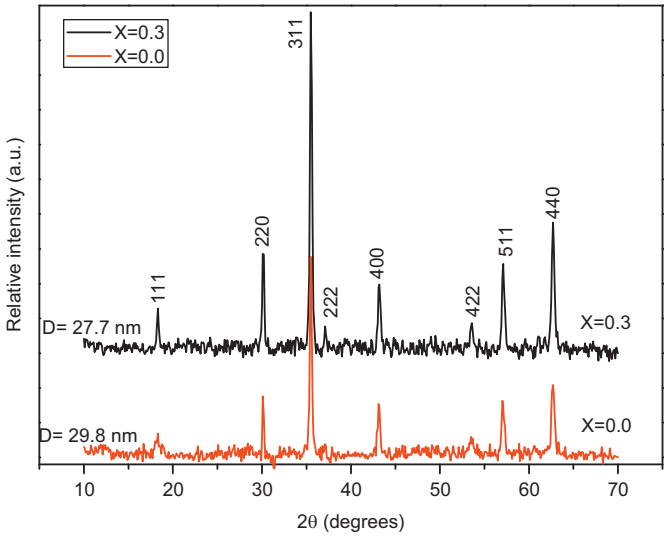

Fig. 1. XRD patterns of chromium doped and undoped samples.

here, D_{XRD} stands for crystallite size; λ is the wavelength of the radiation and β is the full width at half maximum (in radians) centered at 2θ of the most intense peak (in this case it is the peak of [311]).

The lattice parameters have been computed using the d-spacing values and the respective (hkl) parameters from the classical formula given in Eq. (2).

$$a = \frac{\lambda}{2}\frac{[h^2+k^2+l^2]^{1/2}}{\sin\theta} \quad (2)$$

The crystallite size and lattice parameter of the powders were found as 29.8 nm and 8.388 A for pure Co-ferrite and 27.7 nm and 8.386 A for Co-ferrite containing 0.3 mol of chromium. This finding indicated that the synthesized powders had nanosize crystallites and that the substitution of iron ions with 0.3 mol of chromium ions caused a slight reduction in the crystallite size. The inclusion of chromium also led to a slight reduction in the lattice parameter, due to the effective ionic radii of chromium, whose octahedral coordination of 0.615 A is smaller than that of iron, which is 0.78 A as reported by earlier works [32–34].

3.2. FT-IR spectroscopy

Fig. 2 represents the FTIR spectra taken from the samples and PEG. Two main broad metal–oxygen bands are seen in the IR spectra of all spinels, and ferrites in particular. The highest one, v_1, (Fig. 2) generally observed in the range 600–550 cm^{-1}, corresponds to intrinsic stretching vibrations of the metal at the tetrahedral site, $M_{tetra} \leftrightarrow O$, whereas the v_2-lowest band, usually observed in the range 450–385 cm^{-1}, is assigned to octahedral–metal stretching, $M_{octa} \leftrightarrow O$ [33,34]. It is known that Co^{2+} and Cr^{3+} ions preferentially occupy octahedral-site, while Fe^{3+} ions can occupy both octahedral and tetrahedral sites [33,35–37]. In FTIR spectra v_1 (533 cm^{-1}) is slightly shifted towards higher frequency (547 cm^{-1}) with Cr doping as observed in previous work [36]. However, no clear peak due to octahedrally coordinated metal ions has been observed which is expected to be below 400 cm^{-1}. Since our FTIR spectra ranges between 400 and 4000 cm^{-1}, we could not observe octahedral–metal stretching, $M_{octa} \leftrightarrow O$, which is attributed to lower band v_2. This may be due to the broadening of this peak attributed to very small particles of spinel ferrites [31,38].

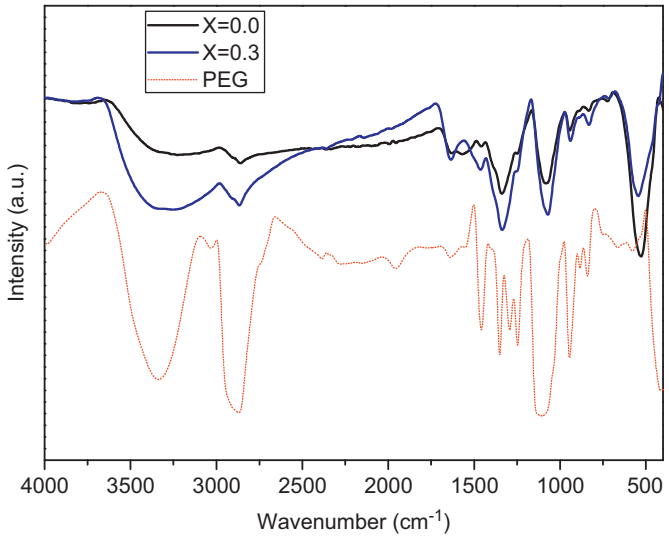

Fig. 2. FTIR spectra of undoped (x=0.0) and doped (x=0.3) $CoFe_2O_4$ nanoparticles synthesized by PEG-assisted hydrothermal method. Dashed line shows the FTIR spectra of PEG.

3.3. SEM measurements

The morphology was examined by scanning electron microscopy (SEM) (Philips, XL30 EDAX model). Fig. 3 shows SEM micrographs of the powders. SEM images reveal that the samples' surfaces exhibit well-defined crystalline nanoparticles of spherical shapes with soft agglomeration. The sample without chromium (Fig. 3a) reveals nanoparticles with a regular morphology and with the presence of soft agglomerations. The powder doped with 0.3 mol of chromium (Fig. 3b) displays homogeneous and finer nanoparticles which are more reactive and hence more agglomerated.

3.4. Magnetic measurements

Fig. 4 shows typical hysteresis loops recorded for undoped and doped samples at some selected temperatures. As it can be seen from the figure, both samples have ferromagnetic behavior at all temperatures. The values of saturation magnetization (M_s) of the samples at room temperature are 56 emu/g (for Co-ferrite) and 48 emu/g (for Cr doped Co-ferrite), respectively. The M_s value for $CoFe_2O_4$ sample is less than the value of saturation magnetization reported for bulk cobalt ferrite (80.8 emu/g) [39]. The M_s value obtained for Cr doped (x=0.3) sample is larger than the values obtained by Toksha et al. [40], Hankare et al. [36] but almost similar to those found by Sun et al. [41] and Han et al. [42]. The magnetization sharply increases at low applied fields but at high field region it increases slowly and does not reach the saturation even at 30 kOe magnetic field. As the temperature decreases, the coercivity values and saturation magnetizations of the samples increase.

The addition of chromium reduced the M_s by 14% and the coercive field by 23%. A decrease in magnetization is expected when chromium is added to the ferrite lattice as observed in earlier reports [27,39–43]. According to Neel's model, the magnetic arrangement of cobalt ferrite consists of two sublattices A and B. The individual moments of A and B sublattices arrange themselves antiparallel to each other, but within A or B sublattice the individual magnetic moments are arranged parallel to one another. So, the magnetic moments of A sublattice and B sublattice cancel each other. The net magnetization of the sample is due to the B sublattice magnetization as the magnetization of the B sublattice is higher compared to the A sublattice. It is

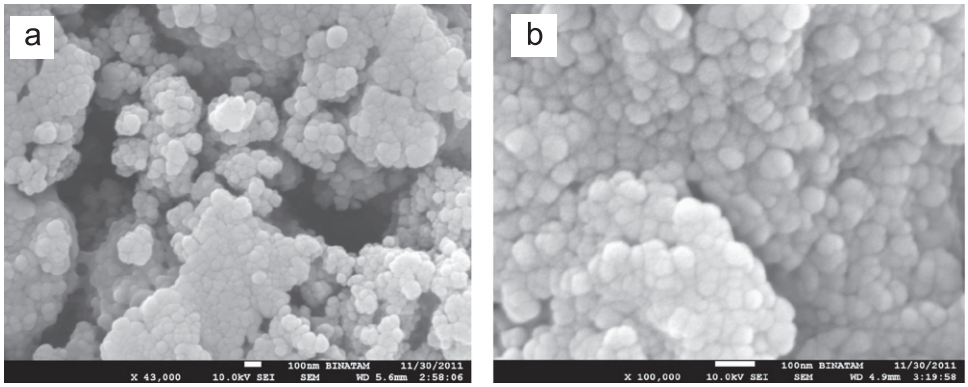

Fig. 3. SEM images of (a) undoped and (b) doped samples.

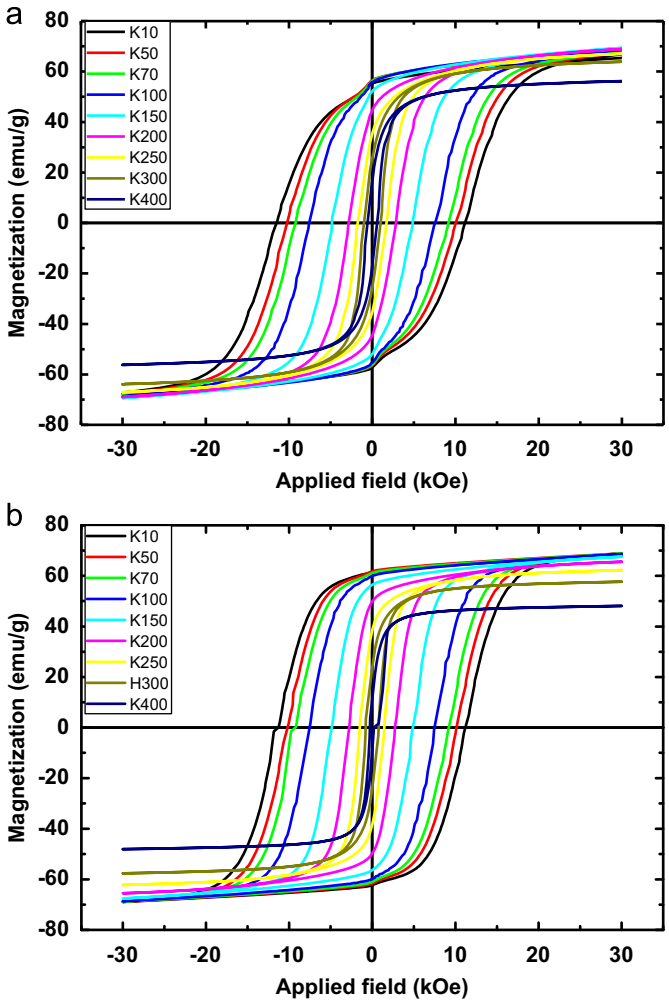

Fig. 4. Hysteresis loops of the samples (a) $CoFe_2O_4$ and (b) $CoCr_{0.3}Fe_{1.7}O_4$ at some selected temperatures.

also known that there are three types of interactions between unpaired electrons of two ions: (i) both ions at tetrahedral A-sites (A–A interaction), (ii) both ions at octahedral B-sites (B–B interaction), and (iii) one at tetrahedral A-site and the other at octahedral B-site (A–B interaction). A–B interaction is much greater than A–A and B–B interactions. The A–B interaction aligns all the magnetic spins at A-site in one direction and all the magnetic spins at B-site in opposite direction. Therefore, the net magnetic moment of the lattice is the difference between the magnetic moments of B and A sublattices, i.e., $M = M_B - M_A$. [44].

When cobalt ferrite is doped with Cr, since paramagnetic Cr^{3+} ion is known to occupy octahedral sites [26,28,44,45] and the density of Fe^{3+} ions at the octahedral B site decreases due to the entrance of Cr^{3+} ions on B sites and thus reducing not only the magnetic moment of the sublattice but also the exchange interaction [26,28,44]. This is due to the fact that the magnetic moment of Cr^{3+} ion (3 μ_B) is less than that of Fe^{3+} ion (5 μ_B) which results in the dilution of the magnetization at the B site and reducing the lattice magnetization. Similar decreases in magnetization and coercivity were reported in different ferrites by Cr^{3+} addition [26,28,45].

The lower value of the coercive field, H_c, indicates that the material was soft ferromagnetic. However, the reduced hysteresis loops and saturation magnetization by the inclusion of 0.3 mol chromium, which in turn lowered the coercive field and softened the material, favoring its application in high-frequency transformers.

Fig. 5 represents the ZFC and FC curves of magnetization of both samples. For cobalt ferrite sample, both ZFC and FC magnetization increase by decreasing the temperature.

As the NPs are cooled to low temperatures in the presence of a magnetic field (FC), the magnetization direction of each particle is frozen in the field direction. While the ZFC magnetization is decreasing, FC magnetization is increasing by decreasing the temperature. Both curves separate and the separation between the ZFC and the FC curves gives an indication that there is a non-equilibrium magnetization below the separation temperature for the ZFC case, and represents the irreversibility temperature, T_{irr}. In general, T_{irr}, represents the blocking–unblocking process of the particles magnetic moment when thermal energy is changed. As the relaxation time of a magnetic particle increases with decreasing temperature, below a certain characteristic temperature called the blocking temperature (T_B) the particles moment appears

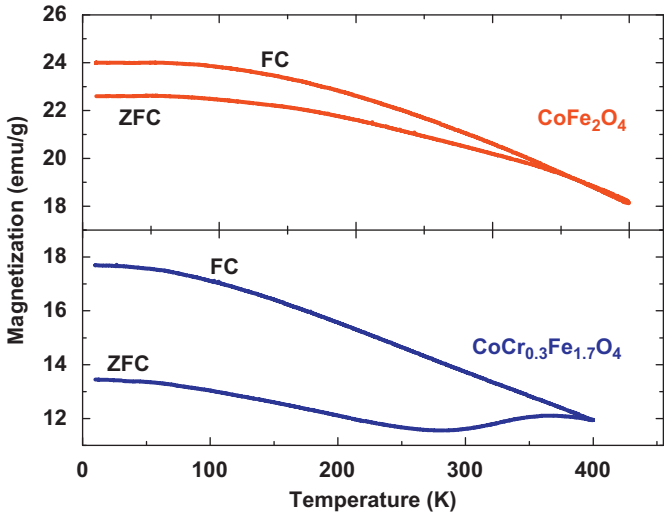

Fig. 5. Temperature dependent magnetizations (M–T graph) of the samples.

blocked with respect to the time scale of the experiment. The difference between T_B and T_{irr} corresponds to the width of the blocking temperature distribution which gives an indication of the narrowness of the anisotropy energy barrier distribution of the particles [46,47]. Below the T_{irr}, the ZFC and FC curves significantly diverge and the sample is in the ferromagnetic state. The divergence in the ZFC–FC magnetization curves below T_B is attributed to the existence of magnetic anisotropy barriers [47].

At temperatures above the blocking temperature, even though the temperature is below the Curie temperature and the thermal energy is not sufficient to overcome the coupling force between neighboring atoms, the thermal energy is sufficient to change the direction of magnetization of the entire crystallite [30,46]. It is also known that fine particles can be easily activated thermally and overcome magnetic anisotropy. Nanoparticles lost their hysteresis property above blocking temperature and magnetic moments follow the same direction with applied magnetic field so that the magnetic moments do not have any remanent magnetization and a hysteresis loop to observe coercive field. The magnetic state for $T > T_B$ is called as superparamagnetic. The blocking temperatures for both samples are above the room temperature and the samples behave as ferromagnetic at the temperatures below the room temperature as seen from M–H curves.

4. Conclusion

In this study, chromium-substituted cobalt ferrite nanoparticles of $CoCr_xFe_{2-x}O_4$ ($x=0.0$, 0.3) have been prepared successfully by using surfactant-assisted hydrothermal route. The structure of the samples was confirmed by FT-IR, XRD and SEM. Crystallite size of the product was found as 29.8 nm for undoped sample and 27.7 nm for doped sample by using line profile fitting of XRD pattern. From magnetic measurements, the saturation magnetization, remanent magnetization, and the coercivity are decreased by Cr doping. The saturation magnetizations of the samples increase with the decrease in temperature.

Acknowledgments

This research was supported by the Fatih University under BAP no. P50011103_Y.

References

[1] M. Yoshimura, K. Byrappa, Hydrothermal processing of materials: past, present and future, Journal of Materials Science 43 (2008) 2085.
[2] R.H. Kodama, Magnetic nanoparticles, Journal of Magnetism and Magnetic Materials 200 (1999) 359.
[3] R.D.K. Misra, A. Kale, R.S. Srivatsava, O. Senkov, Synthesis of nanocrystalline nickel and zinc ferrites by microemulsion technique, Materials Science and Technology 19 (2003) 826.
[4] R.D.K. Misra, A. Kale, B. Hooi, J.Th. DeHosson, Some aspects of nanocrystalline nickel and zinc ferrites processed using microemulsion technique, Materials Science and Technology 19 (2003) 1617.
[5] Z.H. Zhou, J.M. Xue, J. Wang, H.S.O. Chan, T. Yu, Z.X. Shen, $NiFe_2O_4$ nanoparticles formed in situ in silica matrix by mechanical activation, Journal of Applied Physics 91 (2002) 6015.
[6] Y. Köseoğlu, F. Yıldız, B. Aktaş, G.S. Alvarez, M. Toprak, M. Muhammed, Synthesis, characterization and ESR measurements of CoNiO nanoparticles, Physica Status Solidi (b) (2005) 1712.
[7] Y. Köseoğlu, H. Kavas, B. Aktaş, Surface effects on magnetic properties of Fe_3O_4 nanoparticles, Physica Status Solidi (a) 203 (2006) 1595.
[8] J. Popplewell, L. Sakhnini, The dependence of the physical and magnetic properties of magnetic fluids on particle size, Journal of Magnetism and Magnetic Materials 149 (1995) 72.
[9] K. Raj, B. Moskowitz, R. Casciari, Advances in ferrofluid technology, Journal of Magnetism and Magnetic Materials 149 (1995) 174.
[10] D.K. Kim, Y. Zhang, J. Kehr, T. Klason, B. Bjelke, M. Muhammed, Characterization and MRI study of surfactant-coated superparamagnetic nanoparticles administered into the rat brain, Journal of Magnetism and Magnetic Materials 225 (2001) 256.
[11] Y. Köseoğlu, H. Kavas, Size and surface effects on magnetic properties of Fe_3O_4 nanoparticles, Journal of Nanoscience and Nanotechnology 8 (2008) 584–590.
[12] D.K. Kim, Y. Zhang, W. Voit, K.V. Rao, J. Kehr, T. Klason, B. Bjelke, M. Muhammed, Superparamagnetic iron oxide nanoparticles for bio-medical applications, Scripta Materialia 44 (2001) 1713.
[13] E.J.W. Verwey, Electronic conduction of magnetite (Fe_3O_4) and its transition point at low temperatures, Nature 144 (1939) 327.
[14] B. Aktas, FMR properties of epitaxial Fe_3O_4 films on MgO (100), Thin Solid Films 307 (1997) 250.
[15] R.W. Chantrell, G.N. Coverdale, M. El Hilo, K. O'Grady, Modeling of interaction effects in fine particle systems, Journal of Magnetism and Magnetic Materials 157/158 (1996) 250.
[16] V.I. Nikolaev, T.A. Bushina, K.E. Chan, On magnetic properties of superparamagnets in the Curie point region, Journal of Magnetism and Magnetic Materials 213 (2000) 213.
[17] J.-T. Lue, The classical size effect presumes the correction to the dielectric function, The Journal of Physics and Chemistry of Solids 62 (2001) 1599.
[18] M.F. Hansen, S. Morup, Models for the dynamics of interacting magnetic nanoparticles, Journal of Magnetism and Magnetic Materials 184 (1998) 262.
[19] D. Carta, M.F. Casula, A. Falqui, D. Loche, G. Mountjoy, C. Sangregorio, A. Corrias, A structural and magnetic investigation of the inversion degree in ferrite nanocrystals MFe_2O_4 (M=Mn, Co, Ni), Journal of Physical Chemistry C 113 (2009) 8606–8615.

[20] N. Kasapoğlu, A. Baykal, Y. Köseoğlu, M.S. Toprak, Microwave-assisted combustion synthesis of $CoFe_2O_4$ with urea and its magnetic characterization, Scripta Materialia 57 (2007) 441–444.
[21] R.H. Kodama, A.E. Berkowitz, E.J. McNiff Jr., S. Foner, Surface spin disorder in $NiFe_2O_4$ nanoparticles, Physical Review Letters 77 (1996) 394–397.
[22] J. Ding, P.G. McCormick, R. Street, Magnetic properties of mechanically alloyed $CoFe_2O_4$, Solid State Communications 95 (1995) 31–33.
[23] Y. Köseoğlu, A. Baykal, F. Gözüak, H. Kavas, Structural and magnetic properties of $Co_xZn_{1-x}Fe_2O_4$ nanocrystals synthesized by microwave method, Polyhedron 28 (2009) 2887–2892.
[24] C.N. Chinnasamy, M. Senoue, B. Jeyadevan, O. Perales-Perez, K. Shinoda, K. Tohji, Synthesis of size-controlled cobalt ferrite particles with high coercivity and squareness ratio, Journal of Colloid and Interface Science 263 (2003) 83.
[25] K.P. Chae, J. Lee, H.S. Kweon, Y.B. Lee, The crystallographic, magnetic properties of Al, Ti doped $CoFe_2O_4$ powders grown by sol–gel method, Journal of Magnetism and Magnetic Materials 283 (2004) 103.
[26] A.A. Birajdar, S.E. Shirsath, R.H. Kadam, S.M. Patange, D.R. Mane, A.R. Shitre, Frequency and temperature dependent electrical properties of $Ni_{0.7}Zn_{0.3}Cr_xFe_{2-x}O_4$ ($0 \le x \le 0.5$), Ceramics International 38 (2012) 2963–2970.
[27] A.M. Sankpal, S.S. Suryavanshi, S.V. Kakatkar, G.G. Tengshe, R.S. Patil, N.D. Chaudhari, S.R. Sawant, Magnetization studies on aluminum and chromium substituted Ni–Zn ferrites, Journal of Magnetism and Magnetic Materials 186 (1998) 349.
[28] A. Lakshman, K.H. Rao, R.G. Mendiratta, Magnetic properties of In^{3+} and Cr^{3+} substituted Mg–Mn ferrites, Journal of Magnetism and Magnetic Materials 250 (2002) 92.
[29] M. Ajmal, A. Magsood, AC conductivity, density related and magnetic properties of $Ni_{1-x}Zn_xFe_2O_4$ ferrites with the variation of zinc concentration, Materials Letters 62 (2008) 2077.
[30] Y. Köseoğlu, M. Bay, M. Tan, A. Baykal, H. Sözeri, R. Topkaya, N. Akdoğan, Magnetic and dielectric properties of $Mn_{0.2}N_{i0.8}Fe_2O_4$ nanoparticles synthesized by PEG-assisted hydrothermal method, Journal of Nanoparticle Research 13 (2011) 2235–2244.
[31] M. Tan, Y. Köseoglu, F. Alan, E. Şentürk, Overlapping large polaron tunneling conductivity and giant dielectric constant in $Ni_{0.5}Zn_{0.5}Fe_{1.5}Cr_{0.5}O_4$ nanoparticles (NPs), Journal of Alloys and Compounds 509 (2011) 9399–9405.
[32] R.D. Shannon, Revised effective ionic radii and systematic studies of interatomic distances in halides and chalcogenides, Acta Crystallographica Section A 32 (1976) 751.
[33] R.D. Waldron, Infrared spectra of ferrites, Physical Review 99 (1955) 1727–1735.
[34] S. Hafner, The absorption of some metal oxides with spinel structure, Zeitschrift Fur Kristallographie 115 (1961) 331–358.
[35] Maxim V. Kuznetsovy, Quentin A. Pankhursty, Ivan P. Parkin, Self-propagating high-temperature synthesis of lithium–chromium ferrites $Li_{0.5}Fe_{2.5-x}Cr_xO_4$ ($0 \le x \le 2.0$), Journal of Physics D: Applied Physics 31 (1998) 2886–2893.
[36] P.P. Hankare, V.T. Vader, N.M. Patil, S.D. Jadhav, U.B. Sankpal, M.R. Kadam, B.K. Chougule, N.S. Gajbhiye, Synthesis, characterization and studies on magnetic and electrical properties of Mg ferrite with Cr substitution, Materials Chemistry and Physics 113 (2009) 233–238.
[37] Sang Jun Yoon, Seung Hun Lee, Keu Hong Kim, Kyung Soo Ahn, Electrical and magnetic properties of spinel $ZnCr_{2-x}Fe_xO_4$ ($0 \le x \le 1.0$), Materials Chemistry and Physics 73 (2002) 330–334.
[38] M. Sertkol, Y. Köseoğlu, A. Baykal, H. Kavas, M.S. Toprak, Synthesis and magnetic characterization of $Zn_{0.7}Ni_{0.3}Fe_2O_4$ nanoparticles via microwave-assisted combustion route, Journal of Magnetism and Magnetic Materials 322 (2010) 866–871.
[39] D.J. Craik, Magnetic Oxides, Part II, Wiley, London, 1975, p. 703.
[40] B.G. Toksha, Sagar E. Shirsath, M.L. Mane, S.M. Patange, S.S. Jadhav, K.M. Jadhav, Autocombustion high-temperature synthesis, structural, and magnetic properties of $CoCr_xFe_{2-x}O_4$ ($0 \le x \le 1.0$), Journal of Physical Chemistry C 115 (2011) 20905.
[41] G.L. Sun, J.B. Li, J.J. Sun, X.Z. Yang, The influences of Zn^{2+} and some rare-earth ions on the magnetic properties of nickel–zinc ferrites, Journal of Magnetism and Magnetic Materials 281 (2004) 173.
[42] M. Han, C.R. Vestal, Z.J. Zhang, Quantum couplings and magnetic properties of $CoCr_xFe_{2-x}O4$ ($0 < x < 1$) spinel ferrite nanoparticles synthesized with reverse micelle method, Journal of Physical Chemistry B 108 (2004) 583–587.
[43] S. Singhal, S. Jauhar, J. Singh, K. Chandra, S. Bansal, Investigation of structural, magnetic, electrical and optical properties of chromium substituted cobalt ferrites ($CoCr_xFe_{2-x}O_4$, $0 \le x \le 1$) synthesized using sol auto combustion method, Journal of Molecular Structure 1012 (2012) 182–188.
[44] L. Neel, Propriétés magnétiques des ferrites. Ferrimagnétisme et antiferromagnétisme, Annals of Physics 3 (1948) 137.
[45] K.H. Rao, S.B. Raju, R.G. Gupta, R.G. Mendiratta, D.C. resistivity of indium doped Mn-Zn ferrites, Solid State Communications 36 (1980) 777–780.
[46] M. Sertkol, Y. Köseoğlu, A. Baykal, H. Kavas, A.C. Başaran, Synthesis and magnetic characterization of $Zn_{0.6}Ni_{0.4}Fe_2O_4$ nanoparticles via a polyethylene glycol-assisted hydrothermal route, Journal of Magnetism and Magnetic Materials 321 (2009) 157–162.
[47] H. Nathani, R.D.K. Misra, Surface effects on the magnetic behavior of nanocrystalline nickel ferrites and nickel ferrite-polymer nanocomposites, Materials Science and Engineering B 113 (2004) 228–235.